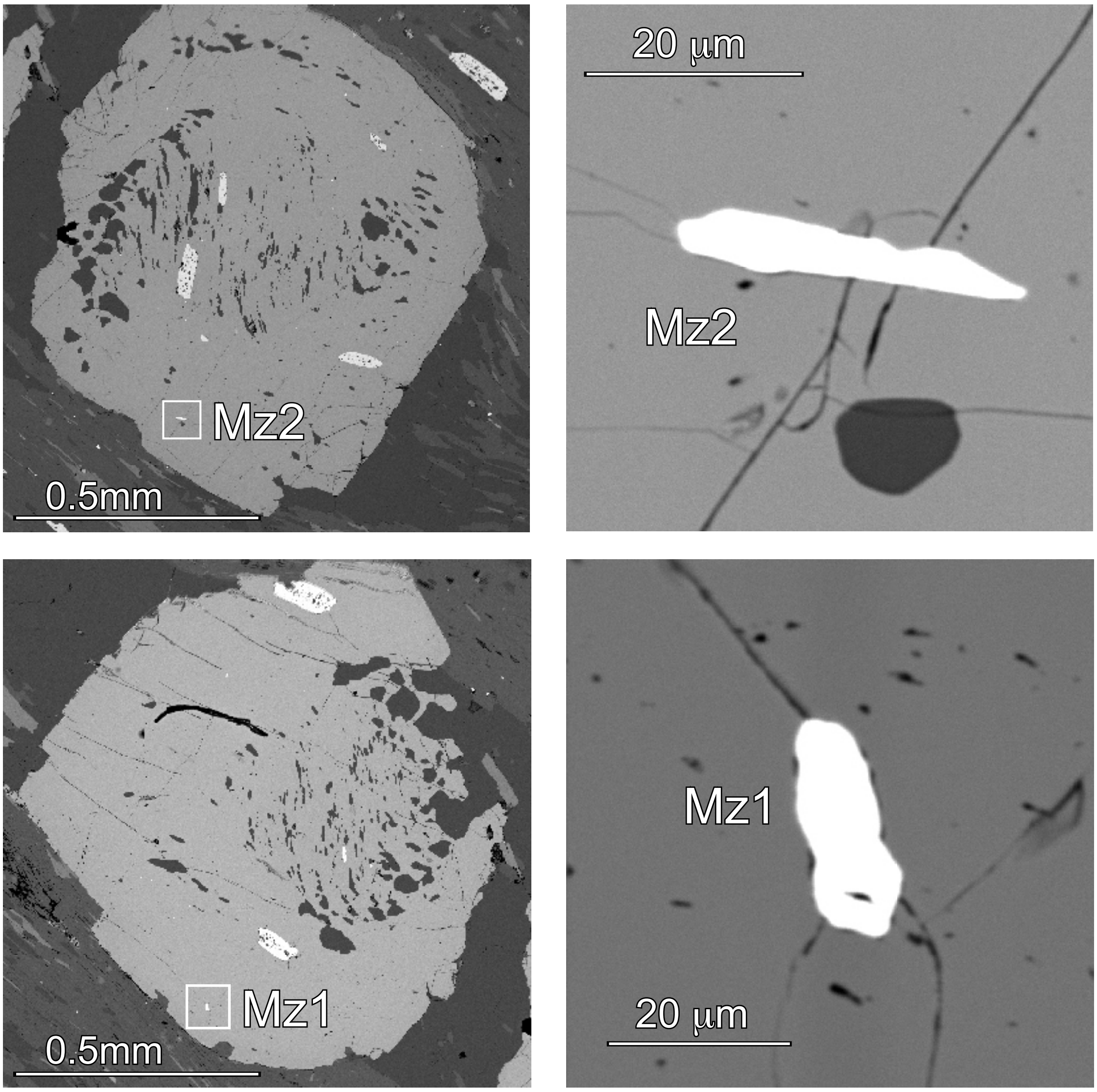

Figure 10. Back scattered electron images showing garnet porphyroblasts from figure 9a and the location of two monazite grains that were dated. Mz1 lies oblique to the foliation containing it and parallel to the foliation in the core.

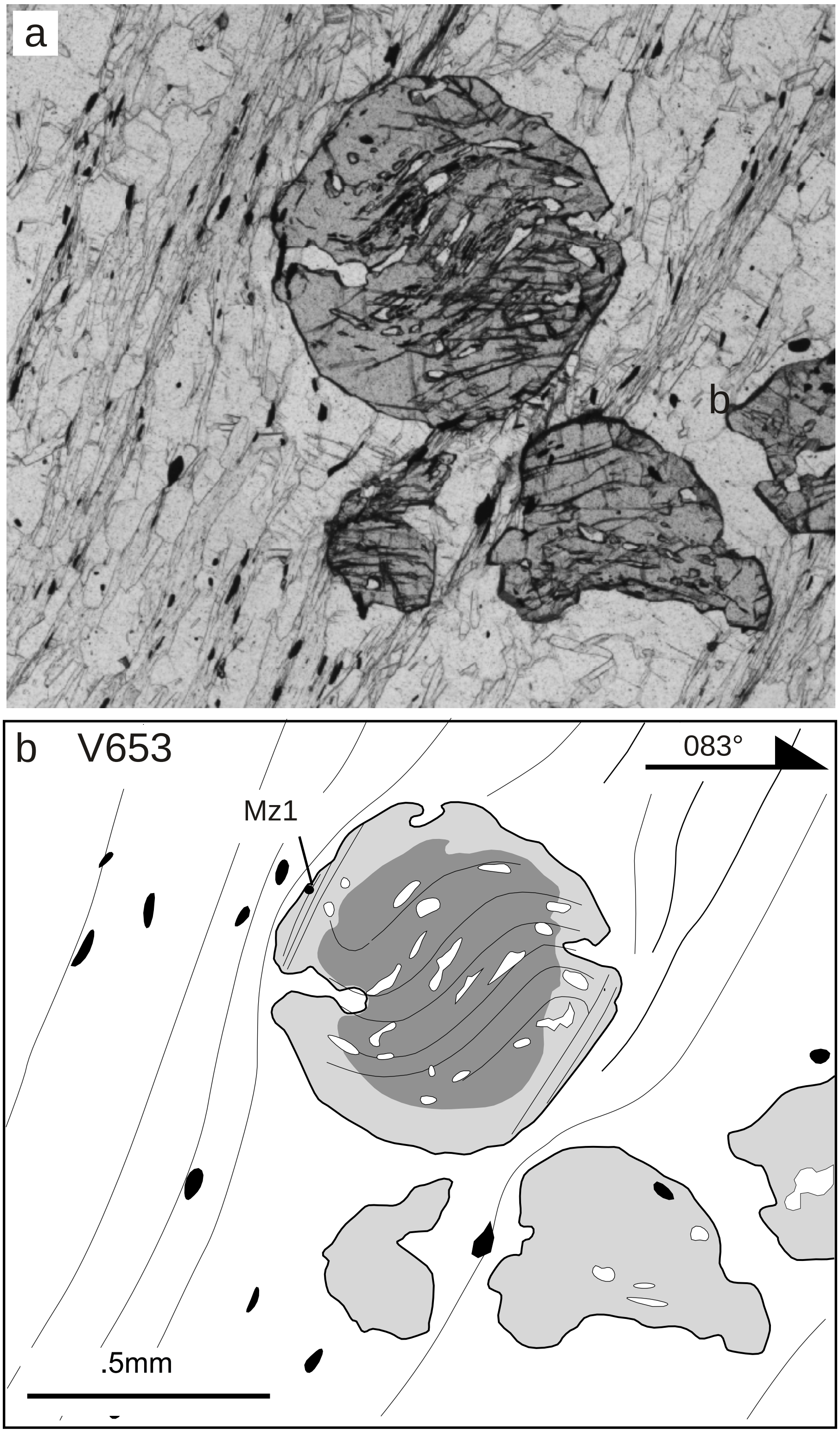

Figure 11. Plane polarized light photomicrograph (a), line diagram (b) and Mg, Ca, Mn and Al compositional zoning maps (c) of a garnet porphyroblast from Sample V653 in a vertical thin-section showing strike and way up (single barbed arrow) and scale bar shown in (b). The location of monazite grains within foliations preserved as inclusion trails in the cores and rims of garnet porphyroblasts and in the matrix are shown in (b). This sample contains FIA set 3 in the core of garnet porphyroblasts but monazite grains are only present in porphyroblast rims and the matrix.

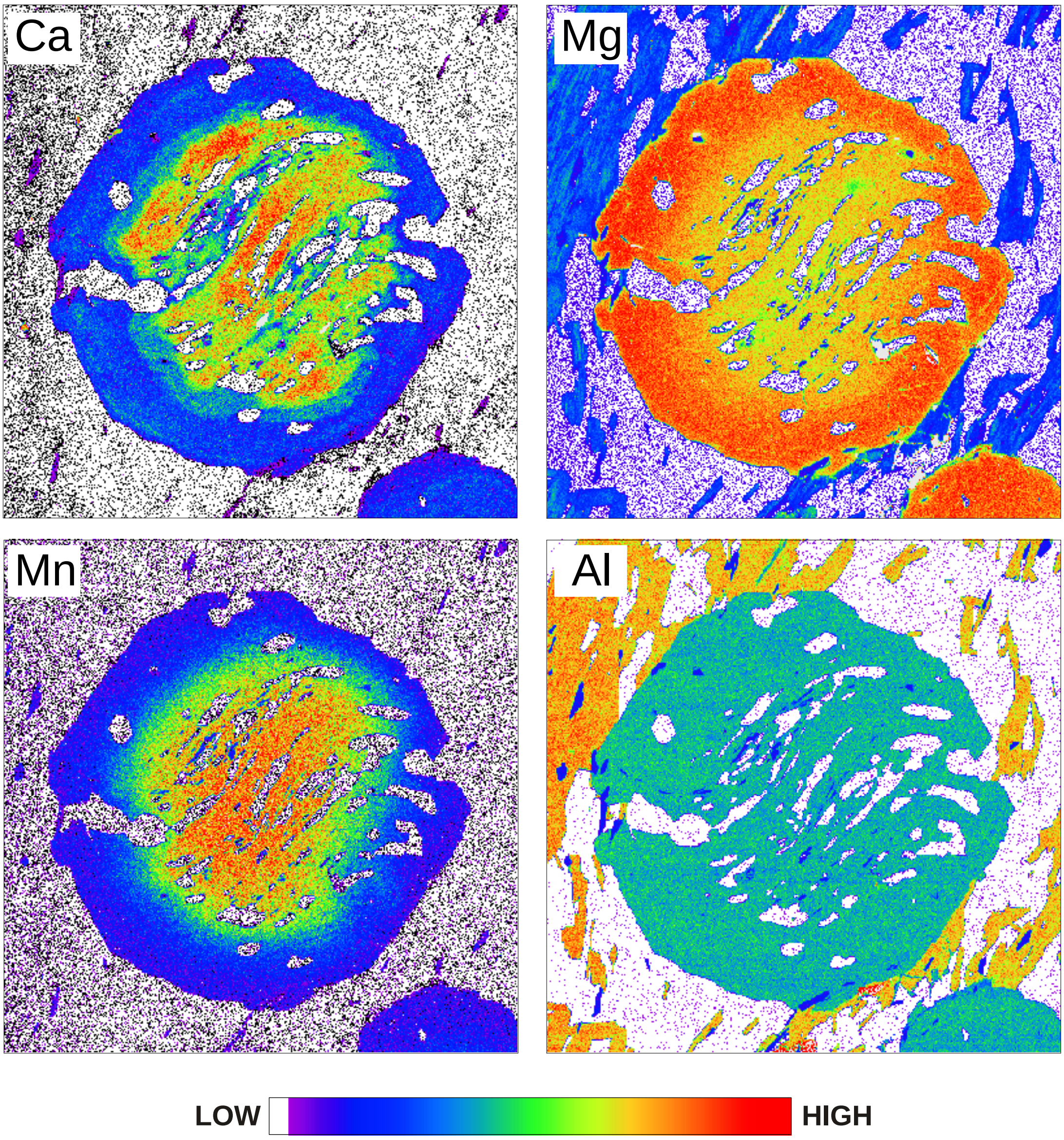

Figure 11c. X-ray compositional maps (Mg, Ca, Mn and Al) for the garnet porphyroblast from sample V653. Colors represent releative concentrations.

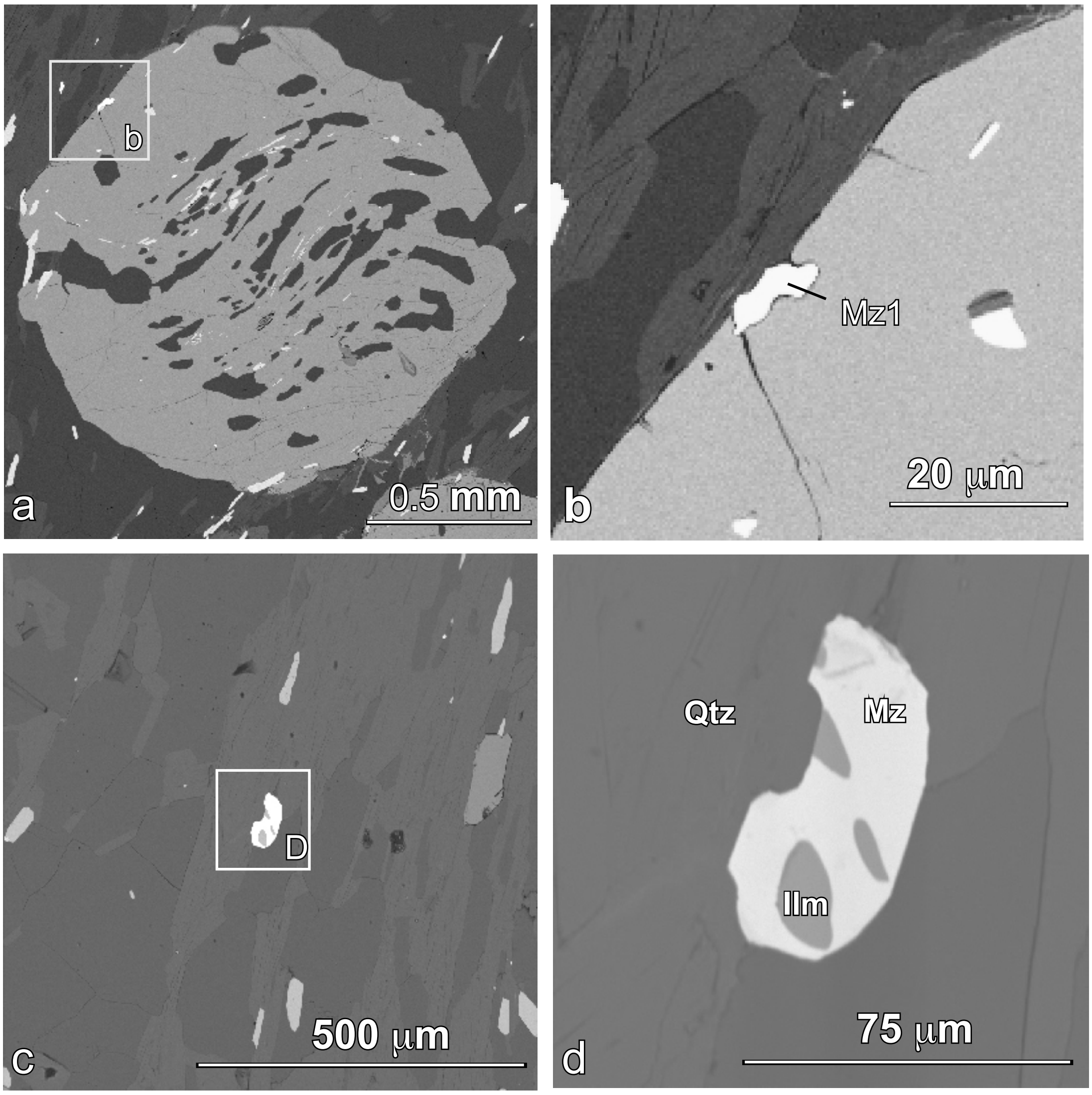

Figure 12. Back scattered electron image of garnet porphyroblast shown in figure 11A, showing enlargement of monazite grain (b) in location marked in boxed area in (a), a monazite grain in the matrix (c) and an enlargement of this monazite grain (d) as it contains rutile inclusions that define a foliation.

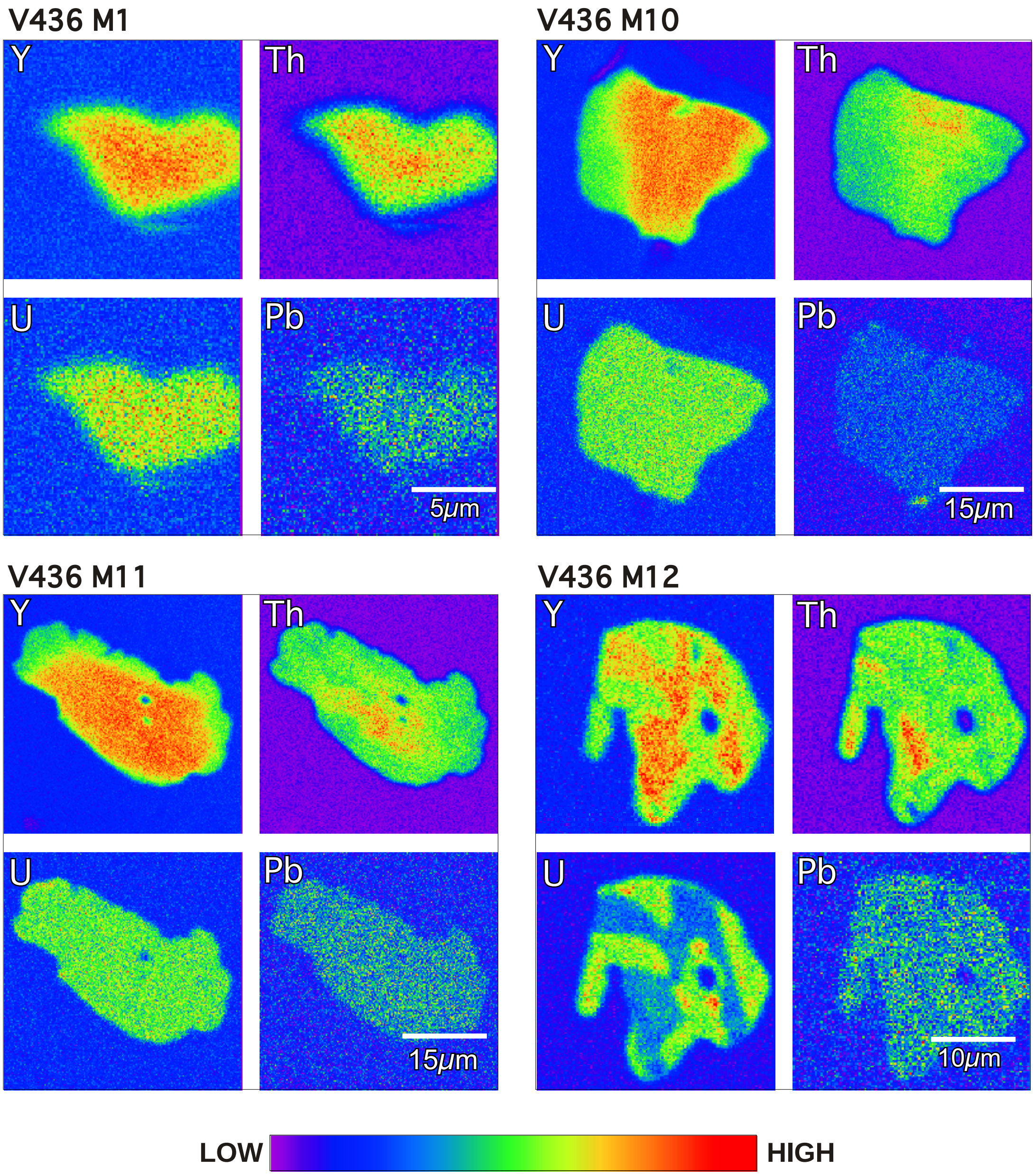

Figure 13. X-ray compositional maps of four monazite grains from Sample V436A showing their Y, Th, U, and Pb contents. As in the garnet composition maps colors represent relative concentrations.

Figure 14. Graphs for 4 samples showing a normal distribution probability curve (unfilled with fine lines) calculated for the mean and standard deviation of each monazite grain from several analyses. Also shown as a bold line is a total sum probability curve calculated for each sample from these normal distribution probability curves. This summation of all of the smaller curves does not include the curves with a gray fill color. The latter curves are plots of the normal distribution probability curve for the weighted average ages (with error ranges calculated at the 2 sigma level of confidence) shown on the side of each plot. These weighted average ages were calculated for all the monazite grains separated according to FIA and whether they lie in the core, median or rim of a given garnet porphyroblast, or the matrix as indicated.

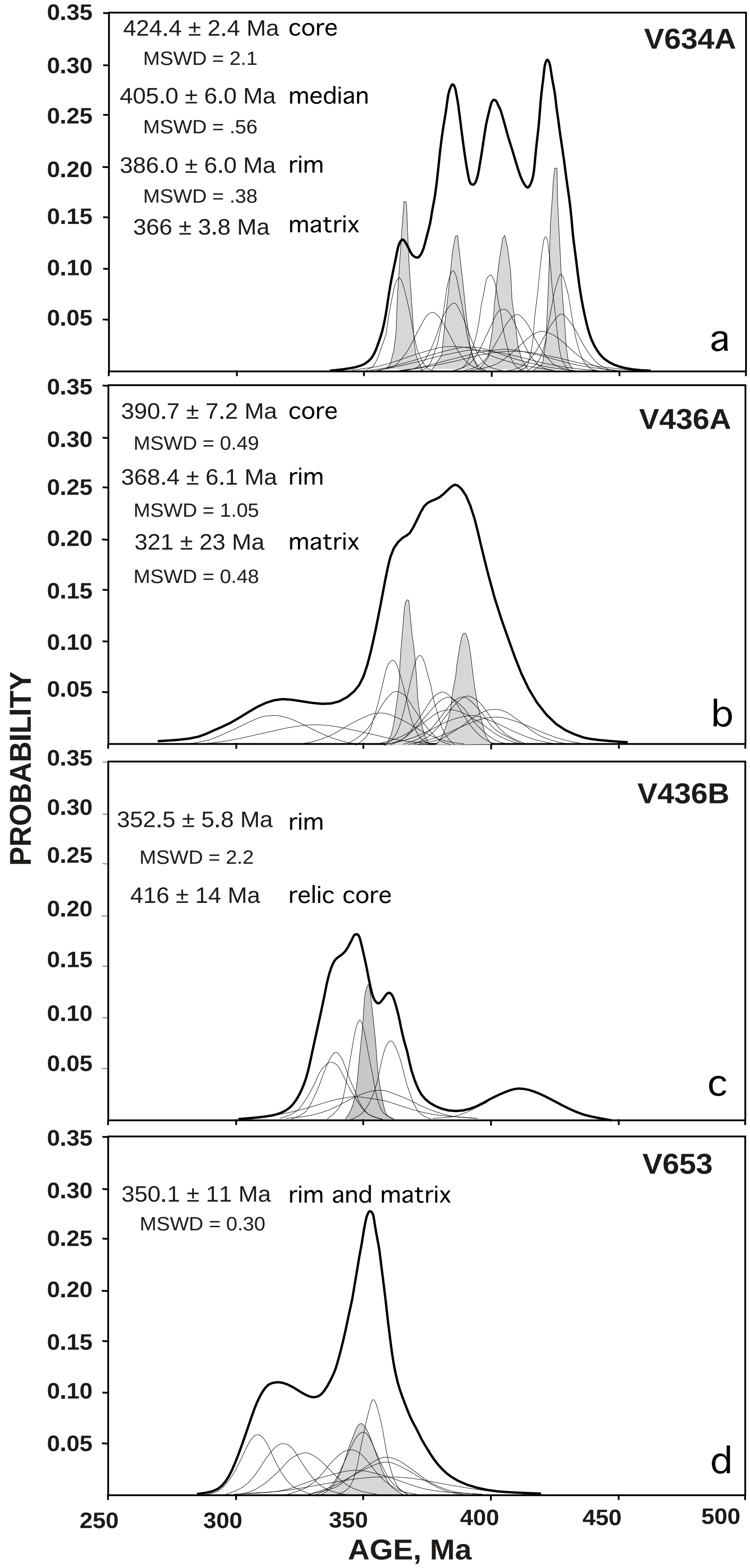
PROBABILITY
AGE, Ma
V634A
424.4 ± 2.4 Ma core
MSWD = 2.1
405.0 ± 6.0 Ma median
MSWD = .56
386.0 ± 6.0 Ma rim
MSWD = .38
366 ± 3.8 Ma matrix
a
V436A
390.7 ± 7.2 Ma core
MSWD = 0.49
368.4 ± 6.1 Ma rim
MSWD = 1.05
321 ± 23 Ma matrix
MSWD = 0.48
b
V436B
352.5 ± 5.8 Ma rim
MSWD = 2.2
416 ± 14 Ma relic core
c
V653
350.1 ± 11 Ma rim and matrix
MSWD = 0.30
d
0.35
0.30
0.25
0.20
0.15
0.10
0.05
250
300
350
400
450
500

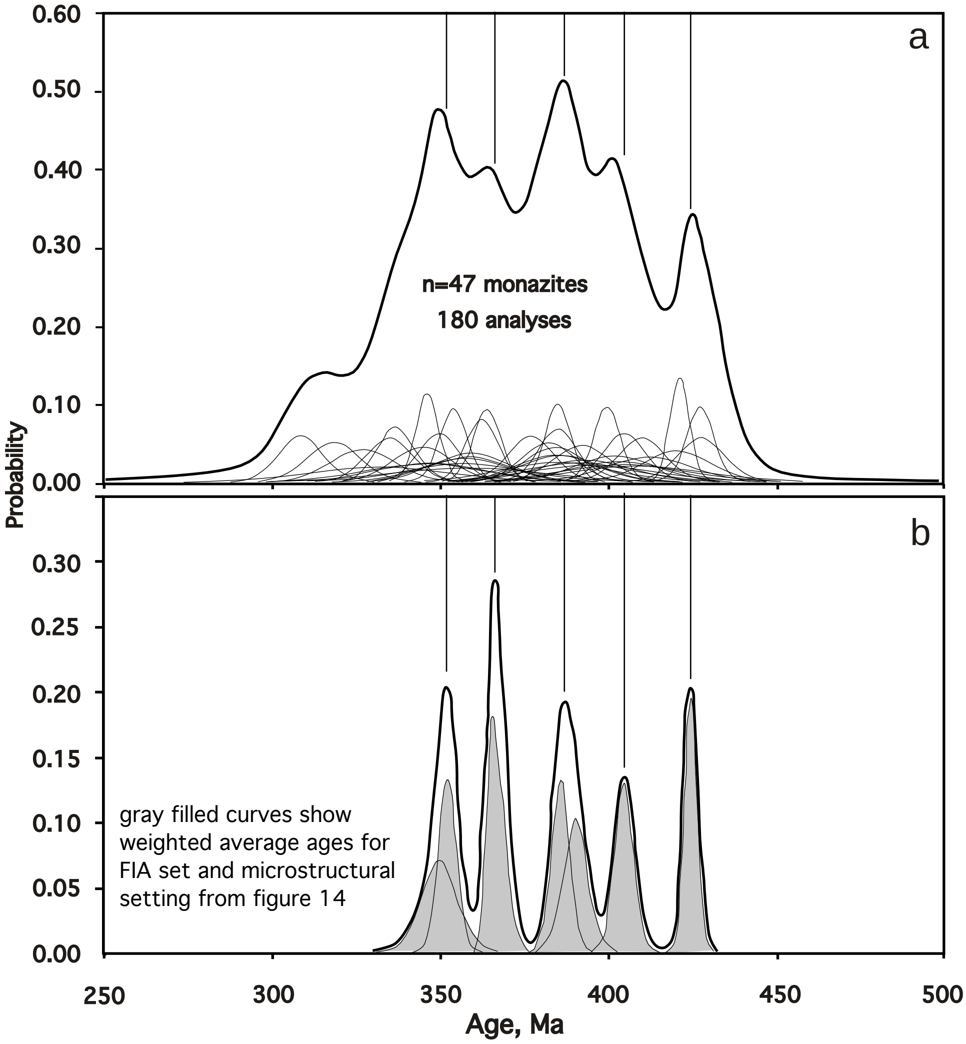

Figure 15a and b. (a) Total probability density (heavy line) curve derived from the sum of probability curves of 47 ages(light lines) of individual monazite grains obtained from the four samples. This can be compared with the individual sample curves in figure 14 and shows that the ages calculated based on FIA and microstructural setting are reflected in the total distribution. (b) Total probability curve (heavy line) derived form the sum of all the probabilty curves ofweighted averages (filled curves) calculted for each sample.

Figure 16. Stages 2 to 5 of the progressive development of crenulation cleavage. (A) stage 2 - crenulation without differentiation. (B) stage 3 - crenulation with development of a differentiated crenulation cleavage (for example, removal of quartz shown) but crenulated cleavage is still connected across zone of differentiation. (C) further development of stage 3 (D) stage 4 - crenulated cleavage disconnected across zone of differentiation by shear or recrystallization of new phyllosilicates along the differentiated crenulation cleavage. (E) stage 5 is destruction of the crenulated cleavage. Stages 1 and 6, which are not shown, are the non-differentiated starting and ultimate foliations. Adapted from Bell (1986). Large arrows indicate bulk shear sense. Small arrows indicate local shear sense between layers/crystals in the matrix. (F) shows nucleation and growth of porphyroblast prior (dark shading) to development of stage 3 of crenulation cleavage development. (G) represents development of stage 4 truncational matrix foliation around the porphyroblast. (H) nucleation of a new stage of porphyroblast growth (dark shading) over portion formed in F, shown in light shading, prior to development of stage 3 of crenulation cleavage development . (I) development of a truncational matrix cleavage from H to stage 5 or 6. (J) growth of 3rd stage of porphyroblast growth prior (dark shading) to stage 3 of crenulation cleavage development with preservation of stage 3 in the strain shadow and stage 4 or 5 in the matrix away from the porphyroblast.

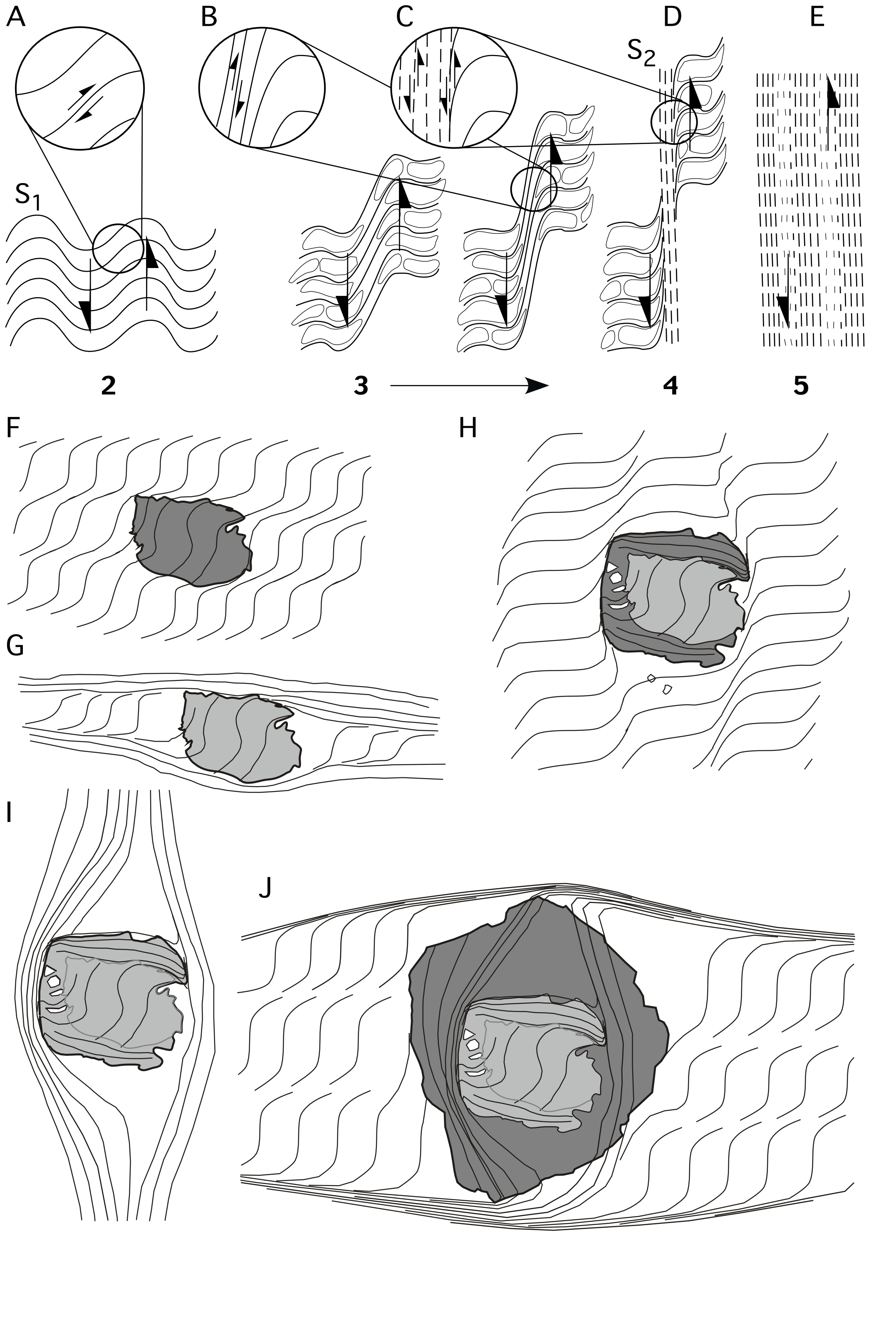
A
B
C
D
E
S2
S1
2
3
4
5
F
H
G
I
J

Figure 17. Sketches showing several stages in the development of the garnet porphyroblast microstructure shown for sample V634A in Figure 5. Dark gray shade indicates portions of porphyroblast that have just grown. Light gray shade indicates portions that grew earlier. The 430 Ma inclusion trails with a preserved Set 1 FIA were crenulated during growth of the garnet that accompanied the development of FIA set 2 as defined by the curvature of the inclusion trails in the core and shown herein (A). The matrix foliation was crenulated to stage 3 of development during the formation of FIA set 3, and resetting monazite ages to 402 Ma (B), before being overgrown by garnet during crenulation by another event as shown in (C). Further deformation during the continued formation of FIA set 3 caused intense shearing and differentiation to stage 4 of crenulation cleavage development against the rim of the porphyroblast at 380 Ma (D). This was overgrown during a younger deformation that also occurred during the development of FIA set 3 (E). The resulting differentiation associated with the horizontal shearing show in E was overgrown by garnet during the development of FIA set 4, which is present in the rim, and resulted in the final geometry shown in (F). This sample contains no evidence for any younger matrix deformation apart from that associated with garnet rim growth during the development of FIA set 4 in F.

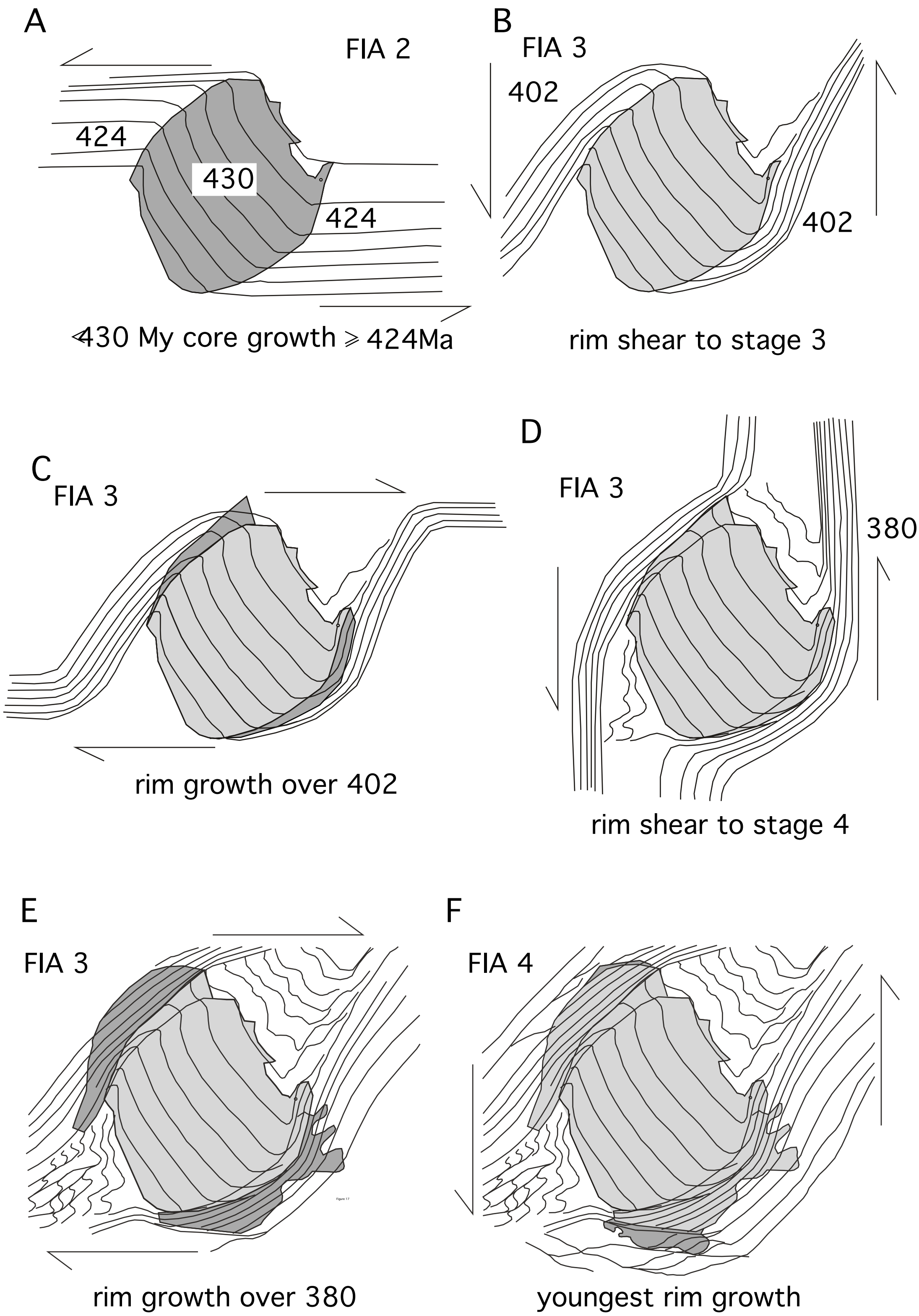
A
FIA 2
424
430
424
<430 My core growth ≥ 424Ma
B
FIA 3
402
402
rim shear to stage 3
C
FIA 3
rim growth over 402
D
FIA 3
380
rim shear to stage 4
E
FIA 3
rim growth over 380
F
FIA 4
youngest rim growth